ASSESSMENT OF AERODYNAMICS AND AERO-ACOUSTICS TOOLS FOR OPEN ROTORS

R. Boisard[*] *- G. Delattre*[*] *– F. Falissard*[†]

ONERA, 29 avenue de la division Leclerc, 92322 Chatillon, FRANCE

ABSTRACT

Counter rotating open rotors have already proven their ability to reduce environmental impact compared to turbofan engines with respect to CO_2 reductions. Nowadays it is more a matter of optimizing this gain in efficiency while keeping the noise level under future certification constraints. The design of such optimized counter rotating open rotors can only be possible if reliable numerical tools are available. In this paper, an assessment of ONERA aerodynamic and aero-acoustic tools for open rotors is performed using the experimental database generated by TsAGI[1] within the European FP7 program DREAM[2]. Comparison between computation and experiment was performed for various levels of modelization (lifting-line method, steady and unsteady CFD) at various Mach numbers around take-off conditions and different rotational speeds. Assessment of aero-acoustic tools was also investigated since noise emission is extremely critical in take-off condition.

NOMENCLATURE

D	propeller diameter, m	τ	thrust coefficient, $\frac{T}{\rho_0 n^2 D^4}$ ‡
Ω	rotational velocity, rad/s	Pt	total pressure, Pa
V_0	advancing speed, m/s	$\underline{U}$	velocity vector, m/s
n	propeller revolution frequency, $\frac{\Omega}{2\pi}$, Hz	W	vorticity tensor, $\frac{1}{2}\left(\nabla\underline{U} - (\nabla\underline{U})^T\right)$
P	propeller power, W	S	deformation tensor, $\frac{1}{2}\left(\nabla\underline{U} + (\nabla\underline{U})^T\right)$
T	propeller thrust, N	Q	Q criteria, $\frac{1}{2}\left[\|S\|^2 - \|W\|^2\right] > 0$
ρ_0	reference air density, kg/m^3		
χ	power coefficient, $\frac{P}{\rho_0 n^3 D^5}$ ‡		
η	propeller efficiency, $\frac{V_0 T}{P}$		

INTRODUCTION

The considerable increase of pressure to reduce CO_2 emission and the increased cost of fuel has renewed the interest for counter rotating open rotor (CROR) propulsion systems over the past few years. Important studies in the 80's[3] had already shown their ability to reach higher efficiency than traditional high bypass ratio turbofan. However, CROR are still noisier than turbofan engines. Nowadays most research focuses on optimizing their efficiency while drastically reducing noise emission to meet not only existing noise certification levels, but also future ones. The design of such optimized counter rotating open rotors can only be possible if reliable numerical aerodynamic and aero-acoustic tools are available. While some basic aerodynamic computational tools were

[*] Applied Aerodynamics Department
[†] Acoustics Department
‡ Computed with front propeller radius

already validated with experiment at ONERA in the 90's[4], CFD and aero-acoustic methods have greatly improved since then.

This paper describes the assessment of up to date ONERA aerodynamic and aero-acoustic tools for open rotors. This assessment was primarily performed within the European FP7 program DREAM[2]. Part of this program is devoted to the aerodynamics and aero-acoustics of open rotors and within these activities, an important open rotor experimental database was generated by TsAGI[1]. This database provides global aerodynamic measurement (thrust, power) along with local flowfield characterization (boundary layer, propellers outflow) at various Mach numbers around take-off conditions and different rotational speeds. Far-field acoustic measurements were done on a line parallel to the propeller axis. The intent here is to compare measured performances (thrust and power) of each propeller, local aerodynamic characteristics and acoustics to results obtained by different numerical models. Aerodynamic computational tools range from a simple lifting-line tool based on 2D airfoil tables to steady CFD mixing-plane method and unsteady CFD chorochronic method. Acoustic post-processing is done using a Ffowcs Williams Hawkings approach over solid surfaces.

EXPERIMENTAL SETUP

Experimental measurements were conducted by TsAGI in their T104 open section, low speed wind tunnel (Figure 1). The chosen configuration was a 0.6373 m diameter propeller at model scale with 12 blades on the front propeller and 10 on the rear one. Nominal Mach number at take-off condition is 0.25.

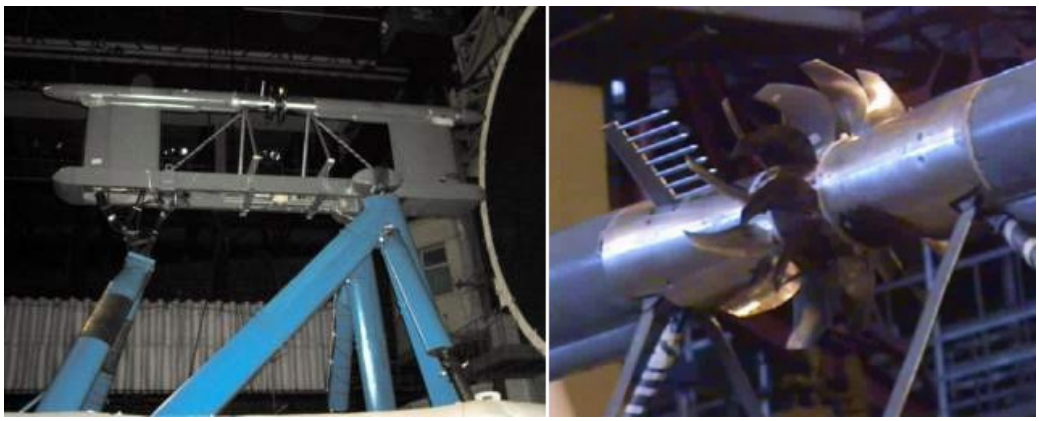

Figure 1: VP107 test vehicles in TsAGI T104 low speed wind tunnel

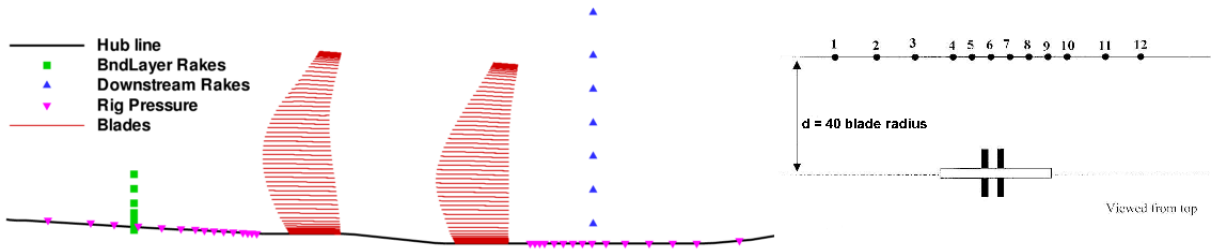

Figure 2: Experimental sensor positioning (aerodynamic on the left, acoustic on the right)

Aerodynamic instrumentation of the test rig gave access to global coefficients for each propeller separately and also to local flow features like test rig pressure upstream and downstream the propellers planes, boundary layer pressure distribution and downstream pressure, temperature and deviation. Positions of the sensors are shown in Figure 2 (left).

Far-field acoustic measurements consist of a line of 12 microphones parallel to the propeller axis placed at 40 radii from the propeller axis, as illustrated in Figure 2 (right).

NUMERICAL METHODS

Tools

Two different tools were used for aerodynamic assessment: LPC2 and elsA. The first one is a fast method based on the lifting-line theory coupled with 2D airfoil tables. This method uses a prescribed wake model coupled with a database of lift and drag coefficients versus angle of attack that are computed on different blade sections for various Mach numbers using a 2D assumption. 3D effects on the actual blade are taken into account using a sweep correction on Mach number and angle of attack. This method was successfully applied at ONERA on various propeller and open rotor configurations in the last decades[4].

The second one is the ONERA 3D RANS solver for complex external and internal flow simulations and for multi-disciplinary applications involving aerodynamics[5]. Recent developments have enabled its use for CROR applications using either a mixing plane or a chorochronic approach. Both methods are relatively efficient in terms of CPU time consumption since they only need to compute one blade channel.

The mixing plane approach is a steady RANS method based on the averaging of the flowfield between propellers and a periodic (in space) boundary condition between blade channels. The chorochronic approach is an unsteady RANS method based on the use of periodic (in time and space) boundary conditions.

CFD computations are performed using a simplified geometry (infinite cylinder, no gap between propellers and test rig) as seen in Figure 3. Meshing strategy and numerical parameters were chosen based on ONERA experience on such computations. The full mesh comprises approximately 5.7 million points for one blade channel. One computation of the nominal point using mixing plane approach was also performed using a highly refined mesh (around 14 million points) but since no significant differences were found, the lightest mesh was used for all the computations in this paper, due to computation time constraint. Mesh extends approximately six blade radii upstream and downstream and five blade radii in the radial direction. All computations were performed at experimental blade pitch angle values. The same grid is also used for the unsteady computations using the chorochronic approach. Numerical parameters are those daily used at ONERA for propeller computations: Jameson centred scheme for spatial flux discretization with 0.5 and 0.032 artificial dissipation coefficients, LussorSca centred scheme for viscous fluxes discretization, backward Euler time discretization, k-ω kok turbulence model with SST correction and Zeng limiter.

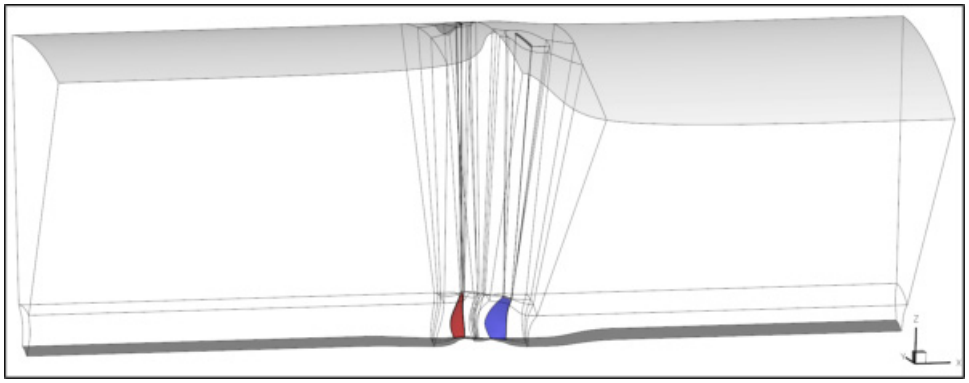

Figure 3: CFD mesh topology

The noise radiated by the open rotor at model scale is computed using the ONERA KIM code[6]. The KIM code is based on acoustic integral methods and can solve the Ffowcs Williams Hawkings

(FW-H) solid or porous surfaces equation as well as the Kirchhoff formulations[7]. The input data used to compute the sound propagation are provided by the unsteady CFD solutions whether on blade surfaces when using the solid formulation of the FW-H equation or on an arbitrary surface encompassing all the noise sources when using the porous surface formulation.

Methodology

First of all a steady computation of the simplified test rig geometry without blade was performed in order to investigate installation effects at nominal Mach number for take-off conditions. The 40 million nodes structured mesh used for this computation is shown in Figure 4.

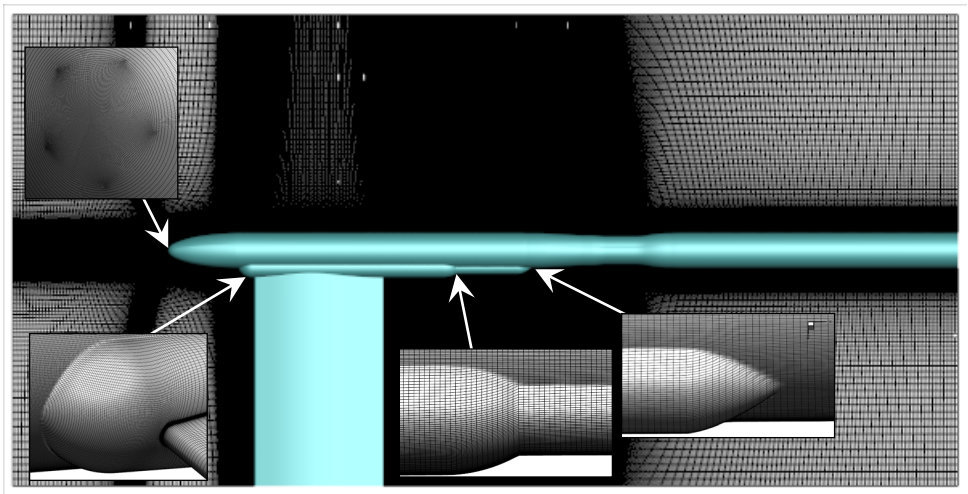

Figure 4: Blades off structured mesh (40 million nodes)

This blade-off computation was validated by comparing test rig pressure distribution between experiment and computation. As seen in Figure 5 upstream pressure distribution is correctly captured. It can also be seen that the pressure on the test rig is not axisymmetrical since the 0° azimuth line and the 90° one do not match exactly. The non axisymmetry of the flowfield is confirmed by the Mach number distribution ahead of the front propeller (Figure 6).

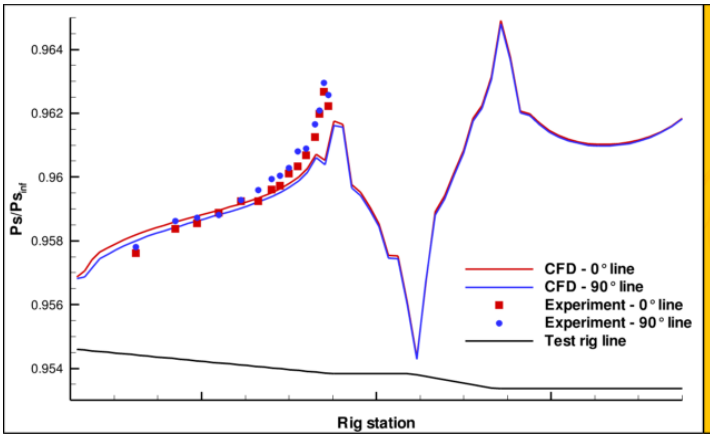

Figure 5: Rig pressure distribution ahead of the front propeller

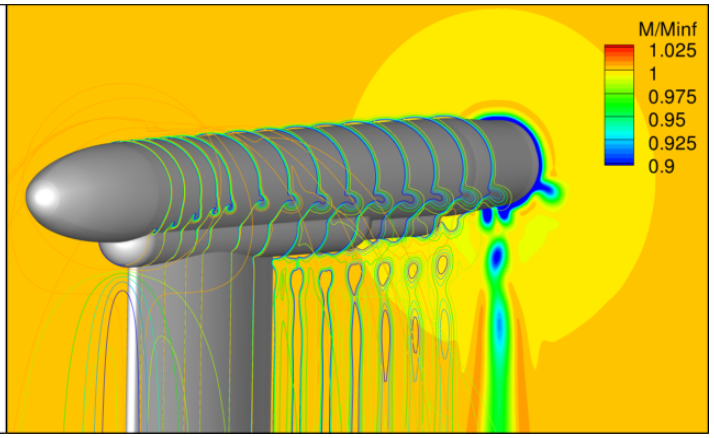

Figure 6: Mach number distribution in the front propeller plane

Due to these installation effects, a methodology has to be set up in order to account for these effects in the aerodynamic computations. The lifting-line method implemented in the LPC2 code was extended in order to handle non axisymmetric flowfield. Flowfield in both propeller planes were extracted from the blade-off computation and used to correct freestream conditions.

Concerning steady CFD computation we have to keep an axisymmetric flowfield since only one blade channel is computed. Therefore only the average perturbation was used. Unfortunately unsteady computation could not be corrected to account for installation effects since it would violate the chorochronic assumption.

AERODYNAMIC ANALYSIS

As well as the nominal take-off point, low speed tests were conducted for a wide range of RPM and free stream conditions in order to investigate Mach number and RPM effects (keeping RPM the same on front and rear propellers). The following sections summarize the analysis of these effects. Note that most aerodynamic computations were performed firstly in the usual way, without accounting for installation effects. A second computation was performed in order to account for installation effects and to outline its benefit when possible.

Take-off Nominal Point

Global coefficients

Thrust, power and efficiency for each propeller are given in Figure 7. It can be seen that the lifting-line method (LPC2) correctly estimates front propeller characteristics but largely underestimates (10 to 15%) rear propeller thrust and power. Surprisingly, mixing plane computations perform worst than the simplest method. Using CFD leads to an overestimation of both thrust and power on both propellers (almost 10% on the front propeller, only 5 % on the rear one). Accounting for installation effects slightly improves CFD results; the lifting-line method results are also improved on the rear propeller, but not on the front propeller. Global coefficients do not feature any major differences between the mixing plane and the chorochronic approaches (both without installation effects).

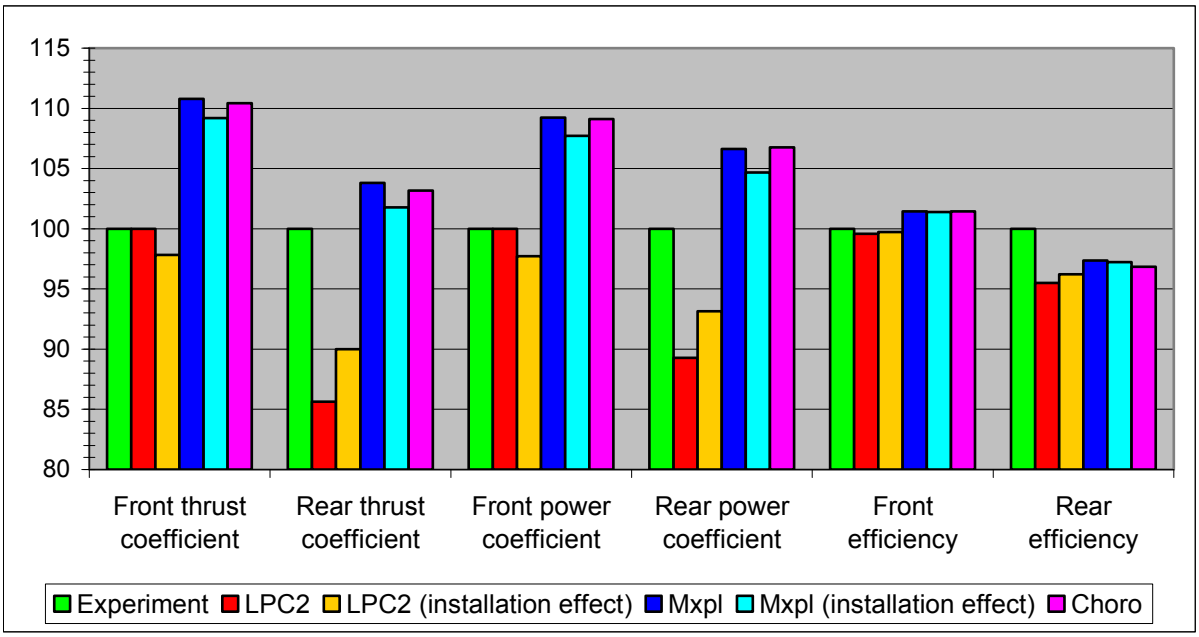

Figure 7: Global coefficients at nominal point (as a percentage of experimental value)

Boundary layer

Figure 8 shows the total pressure distribution in the boundary layer upstream of the front propeller. While accounting for installation effects did not seem to affect global coefficients, they are important when looking at local flow features. The pressure outside of the boundary layer, when accounting for installation effects, recovers experimental values. This is due to the fact that the CFD mesh uses an infinite cylinder, while in experiment the test rig is finite with a bulb upstream, slightly increasing the Mach number around the test rig.

Even if the test vehicles are extremely long compared to the blade diameter, any approximation in the geometry leads to some non negligible differences in the local flowfield.

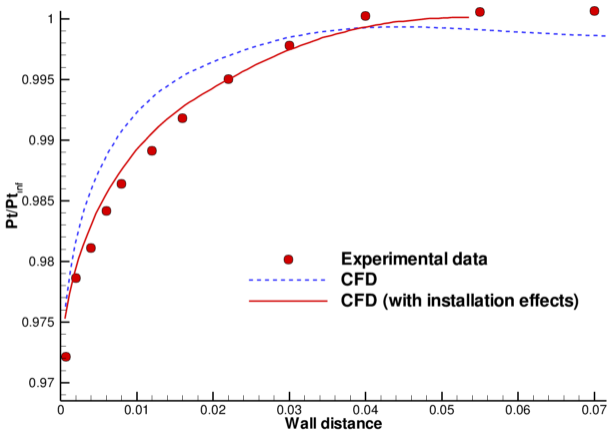

Figure 8: Boundary layer total pressure distribution

Downstream flowfield

Figure 9 shows azimuthally averaged total pressure, Mach number and deviation downstream the rear propeller. Pressure and Mach number are in relatively good agreement between experiment and computation for both steady and unsteady computations. Including installation effects through an axisymmetric perturbation even slightly improves the prediction at the blade root like it was already outlined by the boundary layer analysis. Some oscillations due to the tip vortex interactions are visible on the chorochronic computation, near the blade tip (around 95% radius), on pressure and Mach number distributions but there is not enough measurement from experiment in this area to know if it is physical.

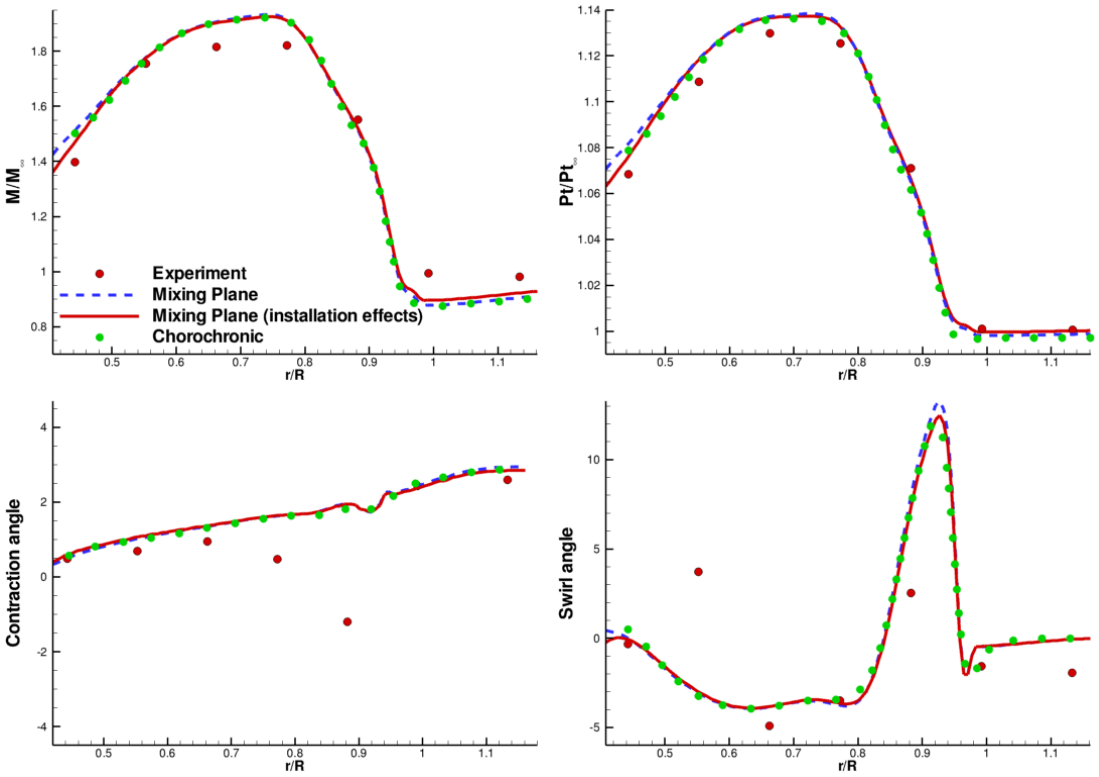

Figure 9: Mean flowfield characteristics downstream the rear propeller

The differences between experiment and computation may be due to the difference in thrust (5 to 10% higher in computation) since computation is performed at experimental blade pitch and not experimental thrust.

The trend of the contraction seems to be also relatively correctly captured. But locally, the important decrease in contraction located around 85% blade radius is largely underestimated by the steady computation (mixing plane). This important change in contraction could be linked to the blade tip vortex. The mixing plane method averages the front propeller wake in front of the rear propeller. Therefore, front and rear blade tip vortex interaction is not correctly captured. The chorochronic computation, which accounts for unsteady interaction, still features results extremely close to mixing plane computation. Such few differences may be due to the fact that unsteady computation underestimates interaction between front and rear blade tip vortex. This underestimation is mainly due to the fact that in the chorochronic computation, the front blade tip vortex intensity drastically decreases as it is convected downstream. It even vanishes near the rear blade trailing edge as seen in Figure 10.

Near the blade root, experiment also features an important variation of swirl while there is no such variation in the computation. This could be linked to a root vortex on the rear propeller that is not captured by CFD. As it can be seen in Figure 10 (Q criteria iso values), vorticity is created at the rear blade root, but in the computation it does not propagate downstream (even on the 4 million points mesh, not shown here, this vorticity is not strong enough to propagate downstream). The small vorticity captured in CFD could be emphasized in experiment due to the actual geometry that features a gap between front and rear propeller and a blade root fillet (Figure 11). Previous propeller computations show that the presence of a gap between front and rear propellers can increase the strength of such a root vortex.

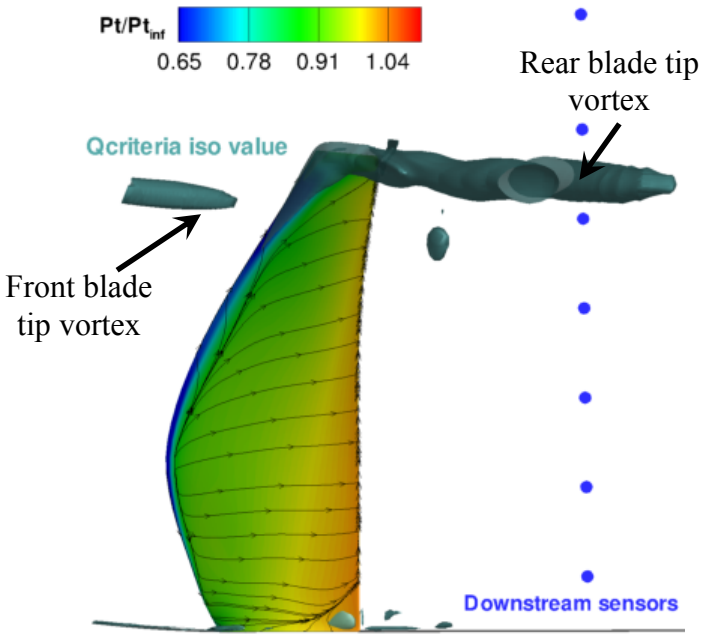

Figure 10: Iso Q-criteria on rear propeller

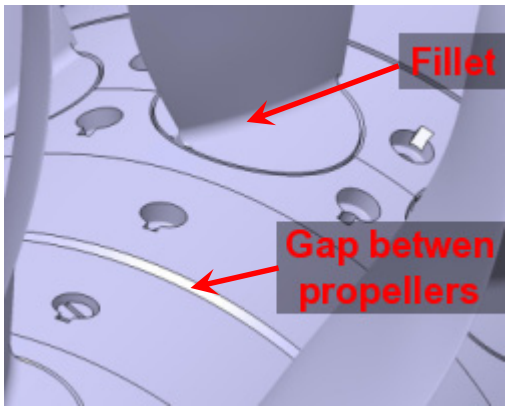

Figure 11: Actual blade root geometry

RPM Effect

In order to investigate RPM effect a set of four tests was performed, starting from the nominal point and decreasing in the mean time both propeller RPMs. Measurements were performed for RPM ranging from 60% to 100% of nominal RPM.

Global coefficients

Figure 12 shows the RPM effect on global coefficients for front and rear propellers using LPC2 with and without installation effects. The overall trends seem to be well captured on both propellers. Absolute values on the front propeller are also well estimated since the error between experiment and computation is less than 10 %, reducing around 5% when accounting for installation effects. Discrepancies seen on the absolute values are much higher on the rear propeller.

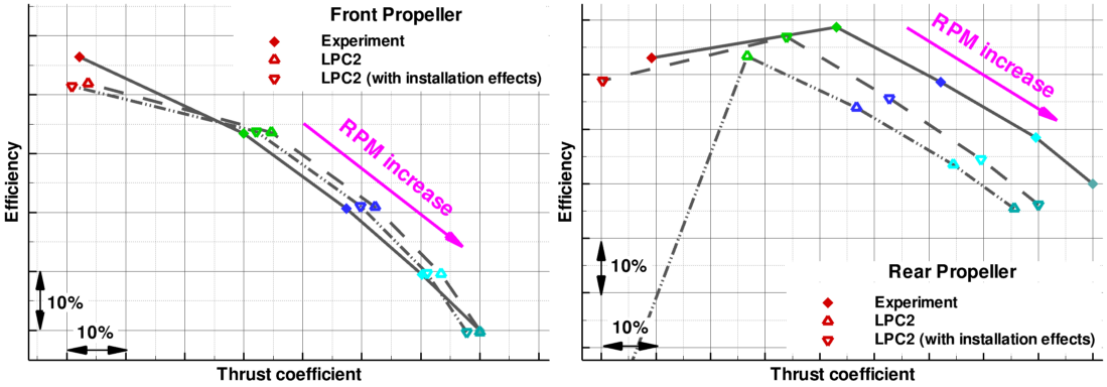

Figure 12: RPM effect on global coefficients with the lifting-line method (LPC2)

Only the low RPM computation (60% nominal RPM) shows important discrepancies on the rear propeller. When looking more into details (not shown here), it can be seen that in such a configuration, the rear blade root is in a deeply stalled condition according to 2D airfoil tables. Blade stall could also be forecast when looking at experiment (loss in both thrust and efficiency) but in a much lower extend.

Accounting for installation effects greatly improves this point. Since LPC2 does not account for any hub line geometry, an important part of the blade does not see the true local Mach number due to the bulb and the hub geometry change. At high RPM, the local flowfield at a blade section is dominated by the RPM and moreover, the blade works far away from the stall region. Therefore a slight change in local Mach number does not affect that much the airfoil characteristics. But at low RPM accounting for the true local Mach number seems mandatory.

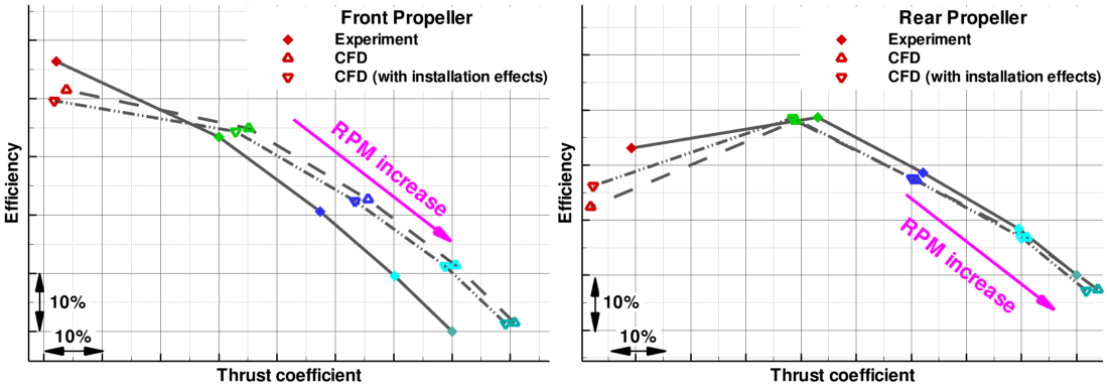

Figure 13: RPM effect on global coefficient with mixing plane approach

Figure 13 shows the RPM effect on global coefficients for front and rear propellers using CFD with and without installation effects. Surprisingly, CFD computation does not seem to be as accurate as the lifting-line method on the front propeller. The increase in efficiency as RPM is decreased is correctly captured, but the absolute values are higher in the CFD computation than in experiment. Accounting for installation effects slightly improves the absolute values but does not

recover all the discrepancy. However, the rear propeller computation seems to be more accurate, with very close values between experiment and CFD. The low RPM point (60% nominal value) features some stall behaviour in both CFD and experiment. Comparison is even improved when using installation effects.

Downstream flowfield

Figure 14 shows the effect of RPM variation on the pressure, Mach number and deviation downstream the rear propeller. Computations seem to accurately capture pressure and Mach number increase as RPM is increased.

Concerning contraction and swirl differences observed at nominal point, they are reproduced over the whole RPM range, except the change in swirl near the blade root. As it was the case for the Mach number variation, the change in swirl near 55% radius is only seen for RPM above 90% of nominal RPM. The fact that it is linked to the RPM and Mach number confirms that it may be due to a root vortex generated by a local flow separation.

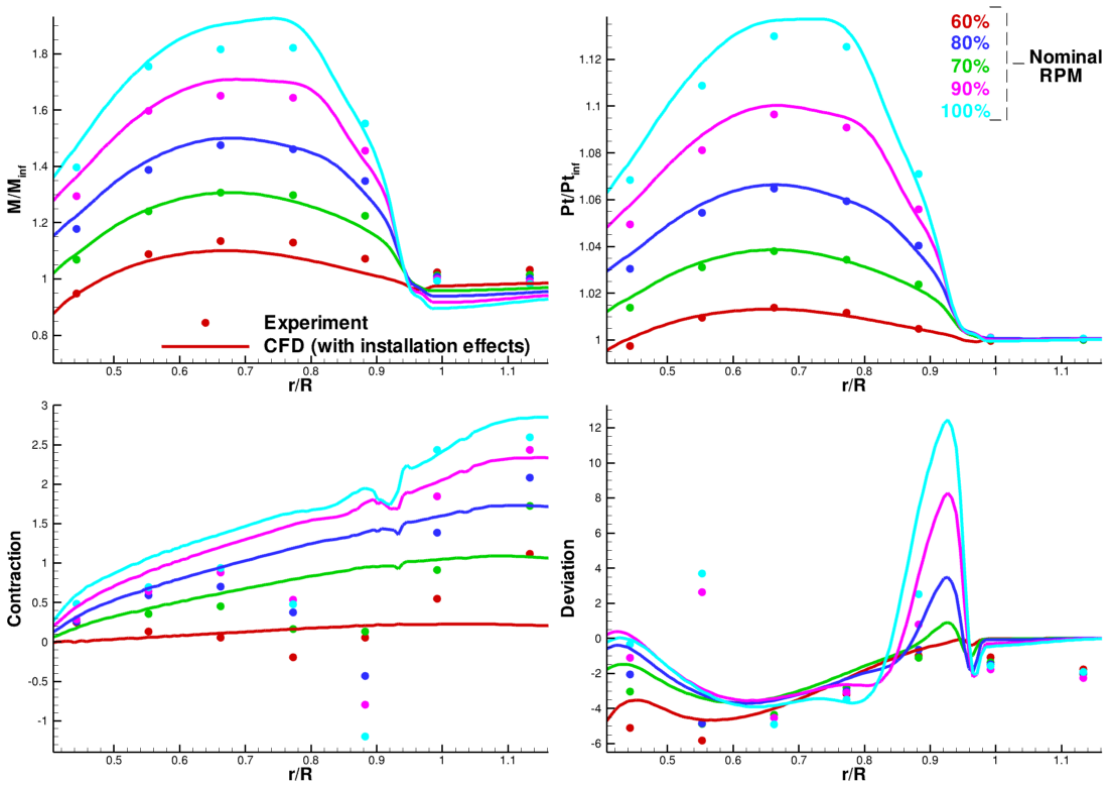

Figure 14: RPM effect on flowfield downstream the rear propeller

ACOUSTIC ANALYSIS

In order to account for the upstream aerodynamic installation effect due to the test rig, the aerodynamic solutions obtained using the lifting-line method have been used as input data for the acoustic computations. Since the lifting line computations provide only blade pressures, the solid surface formulation of the FW-H equation has been used to compute the radiated noise at microphone locations.

Experimental data

The experimental data used for the acoustic study consist in spectra of the acoustic signal recorded at microphone locations. The data are already corrected to account for the background noise and shear-layer refraction of the wind tunnel test section. As it can be seen in Figure 15, the experimental spectra exhibit some scattering of the tones so that the sound pressure levels (SPL)

have been integrated over the tone width in order to be comparable with the SPL acoustic levels computed numerically.

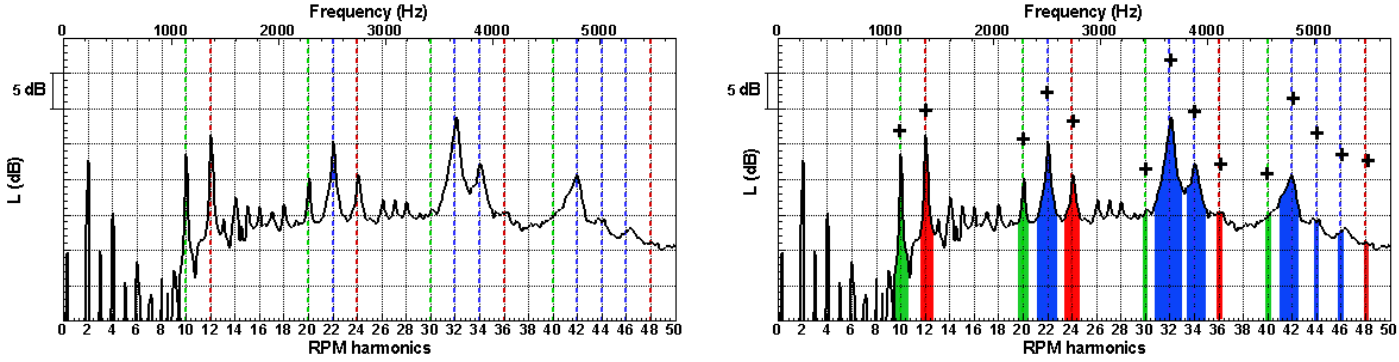

Figure 15: Example of experimental spectra and spectra processing

Acoustic computations

It has been stated previously in this paper that the experimental setup exhibits aerodynamic installation effects that could not be neglected in the aerodynamic computations in order to match the experiments. The same is true for acoustics and the computations have been carried out using the 3 different aerodynamic solutions corresponding to the isolated open rotor, the open rotor with an axisymmetric perturbation of the upstream flow, and the open rotor with azimuthally perturbed upstream flow.

Nominal point

Figure 16 shows the measured and computed noise levels depending on the emission angle for the fundamentals of both propellers and for the first interaction tone.

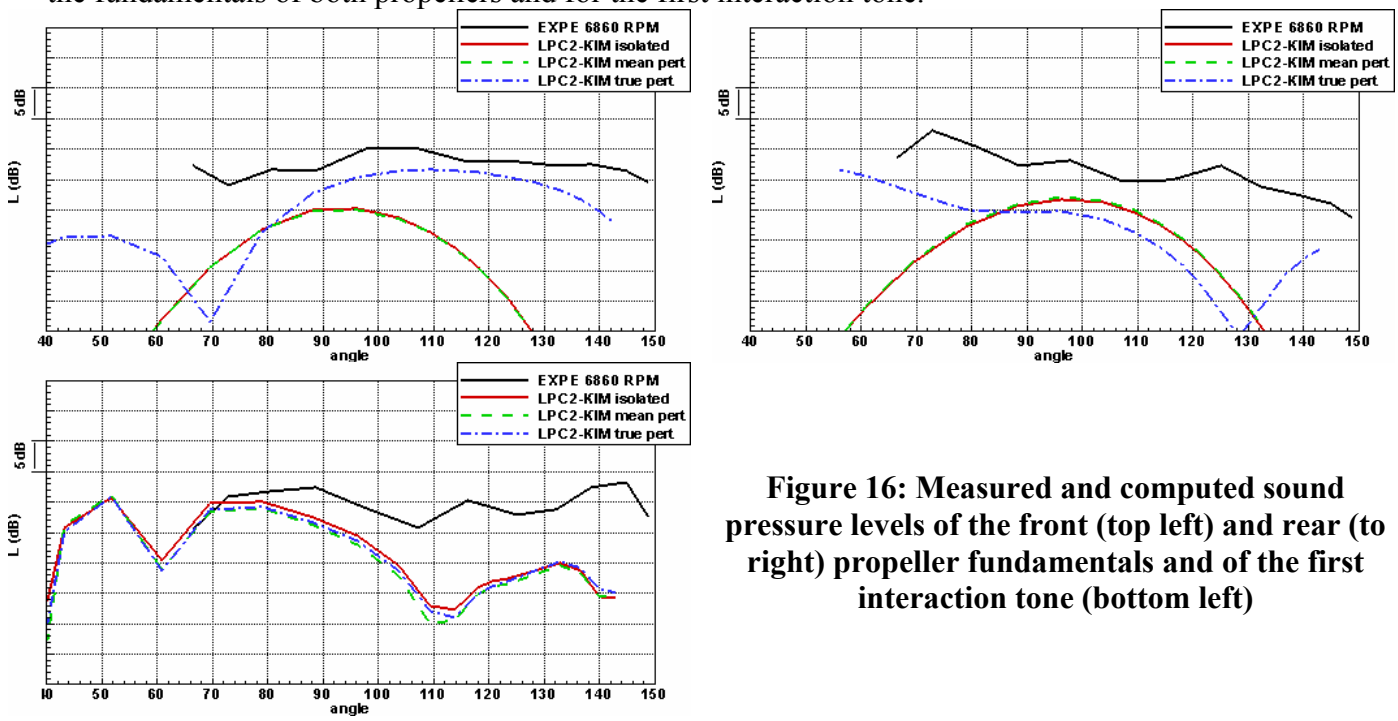

Figure 16: Measured and computed sound pressure levels of the front (top left) and rear (to right) propeller fundamentals and of the first interaction tone (bottom left)

As expected, only the radiated noise computed using the perturbed aerodynamic solution compares reasonably well with the measured values, both in terms of levels and directivity angles. As for the rear propeller, no numerical solution matches the experiment. The directivity of the interaction tones does not depend on upstream installation effects so that all computed solutions provide very similar values. As can be seen, the computed directivity of the first interaction tone

shows some similarity in terms of shape with the measured directivity but the values differ significantly for directivity angles greater than 90 degrees.

RPM effect

Figure 17 shows the effect of the rotation speed variation on the directivities of the tones corresponding to the front propeller fundamental and to the first interaction frequency. The experiment shows that both self propeller noise and interaction noise diminish when the rotation speed decreases. When passing from 6800 rpm to 4000 rpm, the decrease of the front propeller fundamental levels is about 15 dB for all directivity angles and the decrease of the first interaction tone levels varies between 15 and 25 dB depending on the directivity angle. This trend is also present in the acoustic computations based on the aerodynamic solution obtained with a perturbed inflow. The decrease of the computed and measured SPL between 6800 and 4000 rpm are of the same order of magnitude for most rotational speeds.

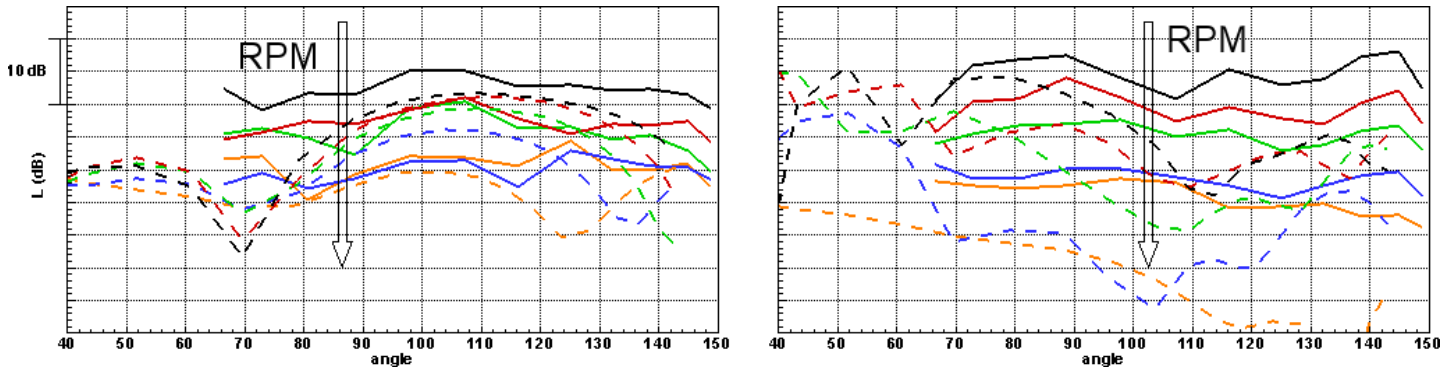

Figure 17: Measured (solid lines) and computed (dashed lines) sound pressure levels of the front propeller fundamental (left) and first interaction tone (right) for rotation speed varying between 6800 rpm and 4000 rpm

CONCLUSIONS

A comparison between experimental results and different ONERA aerodynamic and acoustic predictions was discussed. This comparison was performed on the basis of global performances and local flowfield analysis in take-off conditions.

The lifting-line method shows an important dependency to the 2D airfoil tables that are used. Those 2D tables need to be extremely accurate and the extrapolation of 2D airfoil values to a 3D blade may have to be improved to get the right absolute propeller characteristics. Moreover this method is extremely sensitive to the local flowfield, and accounting for installation effects is mandatory. Even if lifting-line methods are not suitable to get the absolute aerodynamic and acoustic values, all trends are correctly captured. If 2D airfoil table are correctly generated and installation effects are accounted for, it is a valuable tool to compare different designs and it is fast enough to be used in an optimisation loop.

The CFD mixing plane steady approach also features some important discrepancies in terms of absolute global coefficients values. However, local flowfield (downstream flowfield, boundary layer) is relatively well captured. Improved geometry (bulb on upstream cylinder, gap between propellers, blade fillet…) may have to be used in order improve accuracy. Once again, even if absolute values are not fully accurate, trends in terms of Mach number and RPM variations are correctly reproduced. Mixing plane method is very well suited to aerodynamically validate blade shape from lifting-line aero-acoustic optimisation, and could even be used for purely aerodynamic optimisation.

The CFD chorochronic method has the advantage of giving acess to all the unsteadiness of the aerodynamic flowfield. Authors have shown no significant differences compared to the mixing-plane results due to the fact that only mean experimental measurements were available. Moreover,

an important drawback of this method is the impossibility to account for installation effects which has proved to be mandatory with such experimental setup.

The aerodynamic study of the test rig used for experiment has shown pronounced installation effects. The experimental acoustic directivities of the front and rear propeller self noise also exhibit such installation effects. Consequently the computed directivities of the front and rear propeller self noise match better with the experiment when the aerodynamic solution, used as input data, has been computed with an inflow representative of the true perturbation. The acoustic computations also confirm that an azimuthal perturbation of the upstream flow has a negligible effect on the noise related to rotor-rotor interaction.

Finally, only part of the installation effects (axi-symmetric perturbation) was investigated in this study using CFD. A full unsteady computation including the entire test rig is on the way in order to better assess installation effects both from an aerodynamic and acoustic point of view.

ACKNOWLEDGEMENTS

The funding of EU for the DREAM program is fully acknowledged. The authors wish to thank Snecma, CIAM and TsAGI for the discussion of results.

REFERENCES

[1] Central Aerohydrodynamic Institute – Zhukovsky – Russia.

[2] Vali**d**ation of **r**adical **e**ngine **a**rchitecture syste**m**s – http://www.dream-project.eu – contact number 211861.

[3] Hager, R. D. and Vrabel, D., "Advanced Turboprop Project," Technical Report NASA SP-495, 1988.

[4] Gardarein, P., "Calculs aérodynamiques des hélices rapides transoniques", 28eme colloque d'aerodynamique appliquée, Saint Louis, France, 21-23 octobre 1991.

[5] Cambier, L., Veuillot, J.-P., "Status of the elsA CFD Software for Flow Simulation and Multidisciplinary Applications", 46th AIAA Aerospace Sciences Meeting and Exhibit, Reno, Nevada, January 7-10, 2008.

[6] Rahier, G, Prieur, J., "An Efficient Integration Method for Rotor Noise Prediction Starting Indifferently from Subsonically or Supersonically Rotating Meshes". 53rd AHS Annual Forum, Virginia Beach, VA, April-May, 1997.

[7] Ffowcs Williams, J. and Hawkings, D., Sound Generation by Turbulence and Surfaces in Arbitrary Motion, Philosophical Transactions of the Royal Society, Vol. A264, 1969, pp. 321-342.